PEPSI-feed: Linking PEPSI to the Vatican Advanced Technology Telescope using a 450m long fibre

D. P. Sablowski[a], M. Weber[a], M. Woche[a], I. Ilyin[a], and K. G. Strassmeier[a]

[a]Leibniz-Institute for Astrophysics Potsdam (AIP), An der Sternwarte 16, 14482 Potsdam, Germany

ABSTRACT

Limited observing time at large telescopes equipped with the most powerful spectrographs makes it almost impossible to gain long and dense time-series of observations. Ditto, high-time-resolution observations of bright targets with high signal-to-noise are not always possible with large telescopes. By pulling an optical fibre of 450m in length from the Vatican Advanced Technology Telescope (VATT) to the Large Binocular Telescope (LBT) to connect the Potsdam Echelle Polarimetric and Spectroscopic Instrument (PEPSI), allows for ultra-high resolution measurements of bright targets. This article presents the fibre-link in detail from the technical point-of-view, demonstrates it's performance from first observations, and sketches our future plans.

Keywords: high-res spectroscopy, fibre optics, fibre-feed, PEPSI

1. INTRODUCTION

It is common, that large telescopes are used to feed several instruments. This limits the maximum time for observations for each individual instrument. Hence, long and dense time-series of data from a single target is almost impossible to obtain. However, if a high-resolution spectrograph is connected to a medium sized telescope, it is possible to gain data with high quality of bright stars. That is why we have established a 450 m long fibre connection from the Vatican Advanced Technology Telescope (VATT) to the Large Binocular Telescope, to feed the Potsdam Echelle Polarimetric and Spectroscopic Instrument (PEPSI[1]). A good example for science on bright stars is the 0th magnitude binary Capella.[2] To get precise orbital parameters for binaries is of great importance, e. g. for the determination of stellar masses which are very sensitive to the evolutionary status, and on color-surface brightness relation which is important for the calibration of the cosmic distance ladder. Hence, dense time-series observations are essential for these kind of studies.

Three main issues on fibre optics need always be considered when designing fibre-linked instruments: Focal-ratio-degradation (FRD) is the effect of faster output beam compared to the input. It is explained by disturbance of the microstructure between core and cladding as well as macroscopic bending of the fibre itself. Modal noise is the result from interference inside the waveguide which leads to an angular-discrete intensity distribution of the output beam.[3] Transmission is most critical in the blue region towards the near ultra violet in visual applications. Modal noise for long fibres is effectively reduced by the imperfect intersurface between core and cladding which in turn increases FRD. Working with fast input ratios will reduce both modal noise and FRD. The fibre system for PEPSI is designed to work at an input f-ratio of f/3.2 which is near the limit to prevent any losses at the total reflection intersurface between core and cladding due to small beding radii of the fibre cable.

In Sect. 2 we describe the fibre-link from the VATT to PEPSI via the Permanent Fibre Unit (PFU) in detail. We demonstrate the performance of the link with measurements on bright stars in Sect. 3 and draw our conclusions in the last section.

Further author information: (Send correspondence to D.P.S.)
D.P.S.: E-mail: dsablowski@aip.de

2. THE MEASUREMENT CHAIN

We will describe the measurement chain in detail in this section. The light collected by the VATT is coupled into a 200μm circular FBP fibre from Polymicro. The transmitted light after 450 m of fibre is coupled into the octagonal FBP fibre inside the permanent fibre units (PFUs) mounted on the LBT. At the spectrograph input, the output beam is transformed to f/13.9 and injected to the waveguide image slicer. The slicer provides three different modes of spectral resolution.[1]

2.1 Fibre link

We show the optical layout of the fibre-injection in Fig. 1. The f/9 beam provided by the VATT is collimated by a commercial achromatic lens with a focal length of 150mm. The parallel beam passes a beam splitter with an ratio of 99:1 between transmitted and reflected light. The reflected light is directly imaged by a second achromatic lens (50mm focal length) onto the CCD of the guide camera. The transmitted part is imaged by a third lens (100mm focal length) onto the fibre core. The fibre core is positioned behind a reflective pinhole. The light reflected from the pinhole passes the beam splitter again and is reflected by a slightly tilted mirror towards the guide camera. The spot diagrams for all three configurations are shown in Fig. 2

We use a custom 200μm FBPA200240280400 fibre (200μm core, 240μm cladding, 280μm polyimide, and an extra 400μm acrylate for protection) to transport the light from the VATT to the LBT. At the LBT, the fibre is connected to the PEPSI permanent focal station (PFU) at the calibration light input, see Fig. 3. The VATT fibre is attached to an achromatic rod lens to provide an equal output as for the calibration fibre. A mirror can be rotated into the beam and reflects the light to a triplet lens which transforms the diverging beam into a converging beam to match the LBT input. Then using two optional folding mirrors, one of the three available octagonal science fibres can be selected which provide the three different resolution modes. It is also possible to bypass the calibration opitcs to avoid re-imaging losses, in that configuration the fibre is directly attached to the 200μm sky fibre using a fibre-switch inside the left (LBT-SX side) PFU.

The original FBP fiber was directly shipped to the LBT, therefore it was not possible to measure it. However, we measured transmission with a sample FBP fibre and FRD as well as modal noise for a 420m long STU fibre from the same manufacturer. The measurement system used to perform the measurements described below has been decribed elsewhere.[3]

Modal noise measurement Due to interference inside the fibre, the output beam is discrete in space. This intensity structure leads to noise in the spectral measurements. The noise is increased if spatial filters, e.g., input slits are used. It is reduced for fast input beams and towards smaller wavelengths where more modes are excited. Scattering caused by impurities inside the glass and at the interface between core and cladding leads to a decrease of this structure. Hence, it also depends on the length of the fibre. A study[3] on modal noise from short pieces of fibres verified that it is proportional to the number of modes. The modal parameter V is a measure for the number of bound modes $N_M \approx 4V^2/\pi^2$. For circular symmetric fibres, it is given by

$$V^2 = \frac{4\pi^2}{\lambda^2} NA^2 \rho^2, \tag{1}$$

where λ is the wavelength, NA the numerial aperture of the input beam and ρ the radius of the fibre core. If we assume poisson statistics, the signal-to-noise ratio SNR is proportional to the square root of the number of excited modes, $SNR \propto V$. Hence, it increases with decreasing wavelength, fibre core diameter and numerical aperture. The wavelength dependence of the input f-ratio and the maximum number of modes is shown in Fig. 4a and 4b for a core-doped GeO_2 (11.2 mol %) fibre.[4] The f-ratio increases (decreases) towards longer (shorter) wavelength, i.e., it is possible to couple blue light with even faster input f-ratios. Figure 4c shows the number of modes for the same fibre for constant input f-ratio of 3.2.

The overall noise N in the spectrum is given by

$$N^2 = B^2 + M^2 + P^2 \tag{2}$$

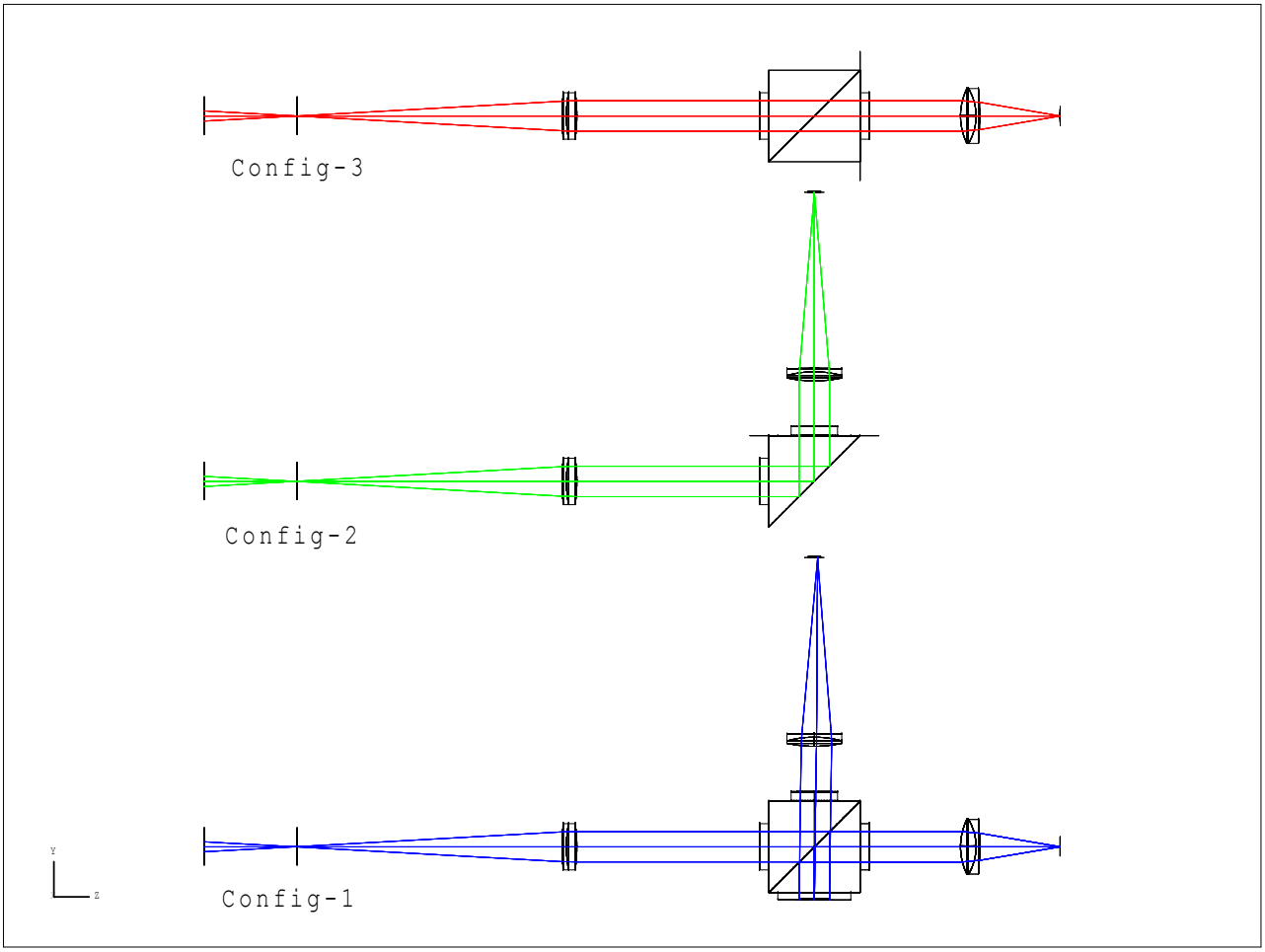

Figure 1: Layout configurations of the fibre link. Configuration 3 shows the path entering the fibre, configuration 2 shows the direct reflected path towards the guider camera and configuration 1 shows the full path reflected at the fibre pinhole and imaged onto the guider camera slightly offset in respect of the direct reflection.

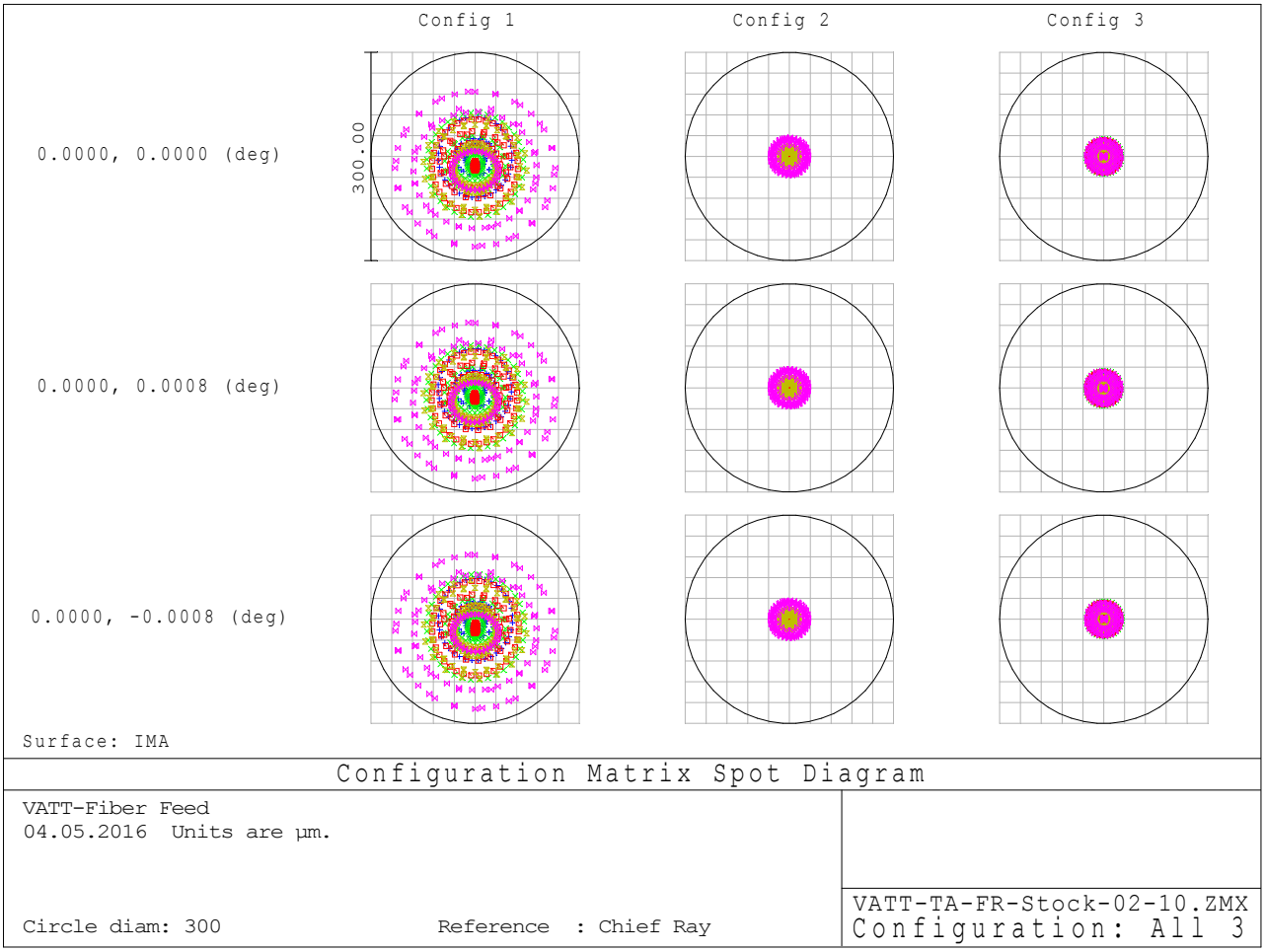

Figure 2: Spot diagram for all three configurations. The circle has a diameter of 300μm. After back-reflection from the pinhole, the beam suffers from stronger aberrations. However, since the direct reflected image is used for guiding and the image quality at the pinhole surface is sufficient, commercial lenses where used.

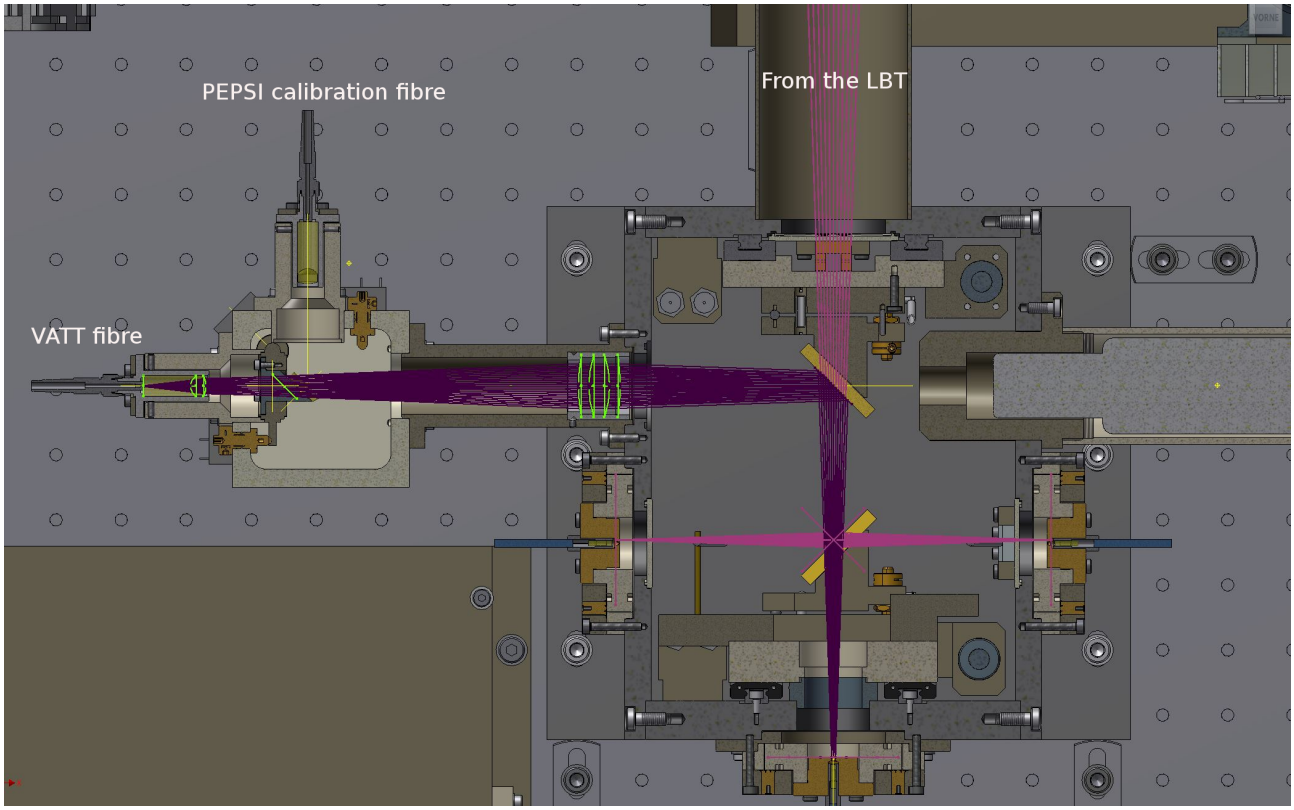

Figure 3: Connection of the VATT fibre (top left) at the calibration input at the PFU. The output is transformed to match the LBT f-ratio and is reflected towards the octagonal science fibres.

the square-sum of the background noise B, the photon noise P and the modal noise M. The background noise was reduced by using an average of ten images. Furthermore, we measured that noise in the mean image and compute the modal noise from the measured overall noise in the spectrum according to

$$M = \sqrt{N^2 - B^2 - P^2}, \tag{3}$$

where we determined P from the count rate in the spectrum. The SNR measurements shown in Fig. 5a have been performed with a Czerny-Turner spectrograph. The spectrograph suffers from astigmatism, which causes the spectrum to expand several times as geometrically expected. Hence, the interference structure of the spectrum is pronounced and well measurable. We have performed the SNR measurements in the spectral region between 674 and 698nm. Resolving power of the spectrograph is 20.000 for a 50μm input slit width and the dispersion is 0.0157nm/pix at a pixel size of 9μm. Hence, we need to note that these measurements are comparable to among themselves, but do not set overall limits.

We measured the SNR of the fibre on and off the spool, which is plotted in the aforementioned figure. The values for the fibre on the spool are higher except for the measurement at f/10 input. For the fast input at f/4 and f/5 the measurements are photon noise limited, i.e., modal noise is not present. However, if these measurements are compared with those in[3] (Fig. 7) modal noise is strongly reduced even for the measurements off the spool, which is the more realistic case. An increase of ≈4.6 is achieved if we compare the value for f/4 input in Fig. 7 for the 200μm circular fibre of the aforementioned paper with our measurements.

Focal-Ratio-Degradation We have measured the 420m long sample of a STU fibre for input f-ratios of 3.2, 4, 5, 7 and 10 and show the results in Fig. 5b. We also plot the relation input f-ratio equal to output f-ratio. The measurements where performed for the six central wavelengths of the cross-dispersers of PEPSI, but there

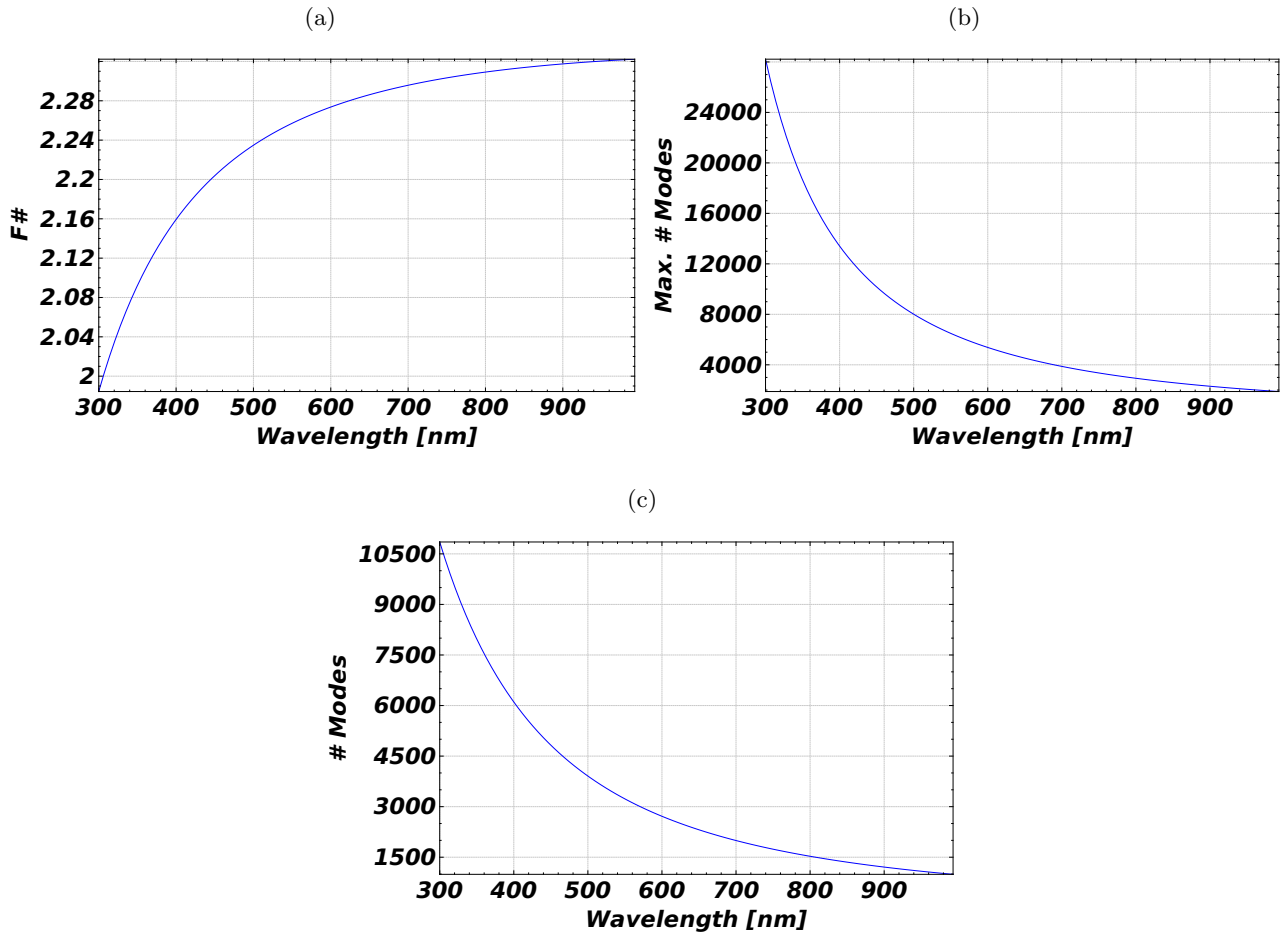

Figure 4: a: Input f-ratio for a core-doped GeO_2 (11.2 mol %) fibre. b: Maximum number of modes calculated with the wavelength dependent f-ratio. c: Number of modes for a constant input f-ratio of 3.2.

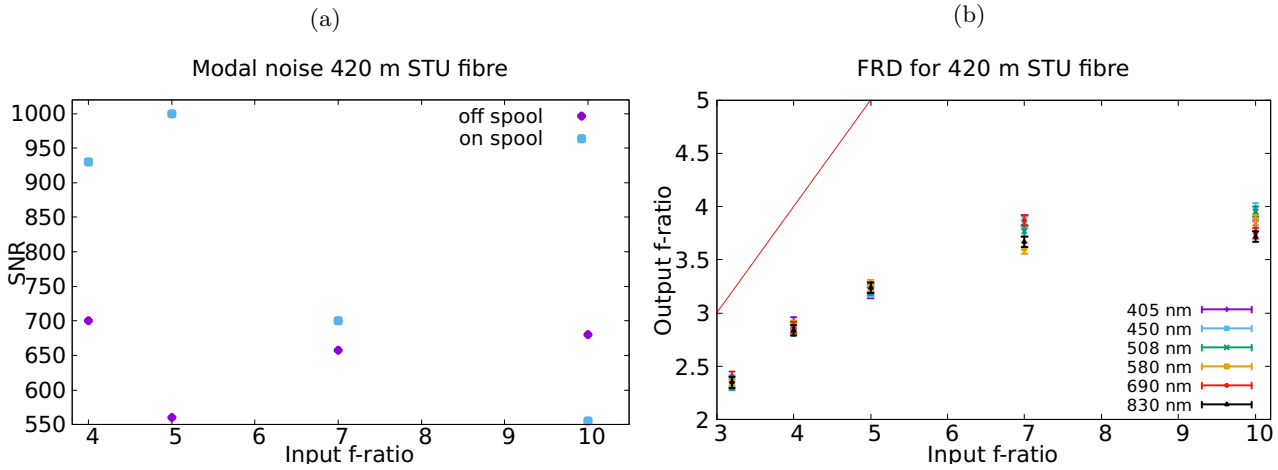

Figure 5: (a) Measured modal noise of 420 m STU fibre on and off the fibre spool; (b) FRD for a 420m long sample of STU fibre. Also shown is the relation input f-ratio equal to the output f-ratio.

is no hint for a wavelength dependence of the FRD. These measurements show strong FRD even for slow input ratios. F/4 input, e.g., yields and output of around F/2.8 which is around 0.3 lower than the ratio in Fig. 10 in.[3]

Transmission In broadband applications in the visual range of the spectrum, transmission is critical in the blue region towards the ultra violet. This is caused by Rayleigh scattering as well as scattering caused by impurities inside the glass and the non-ideal interface between core and cladding. Additionally, absorption caused by the hydroxide anion affects the transmission towards the near infrared. Therefore we have measured the transmission of three different types of fibres and show the results in Fig. 6. The STU sample was 420m long, the FBP sample we used had a length of 50m and the WF fibre was 500m long. We extrapolated the FBP measurements. The data provided by the manufacturer for the WF fibre was for a 200μm core fibre and we performed the measurements with a 72μm fibre.

The measurements where done in the following way. Both ends of the fibre where glued to connectors and polished. We used interference filters (405, 450, 508, 580, 690 & 830nm) with a bandwidth of 10nm to get the transmission in dependence of the wavelength. We measured the throughput of the fibre and at the same time we recorded the fluctuations of the illumination source to correct for them afterwards. Then we cut down a piece of 1m from the sample fibre, connectorized and polished it again and measured the throughput of that short fibre under the assumption that it is only affected by coupling losses. We did not disconnected the other fibre end from the illumination system while preparing the bare fibre end. This was repeated five times for each fibre to get the errorbars as plotted. We conclude for these measurements, that the provided values from the manufacturer are in good agreement with our measurements.

2.2 Guding and PEPSI interface

The PEPSI VATT telescope adapter is equipped with the guiding Basler acA1600-20gm/gc camera which has the Sony ICX274 $1600 \times 1200 \times 4.4\,\mu\text{m} = 7.04 \times 5.28\,\text{mm}$ CCD. The scale factor on the CCD is 0.11 arcsec/pix.

The camera is a GigE Vision closed-source standard interface which requires a 1GB Ethernet link. A separate local computer server Dell R220 is used to provide the high-speed Ethernet link to the camera and hosts the graphical user-interface to the guider application. The PEPSI control program is then linked to the guider GUI via LBTO general-purpose network over an `X11`-forwarding `ssh` socket.

To communicate with the Basler, we use the third party open-source software library Aravis (`wiki.gnome.org/Projects/`
which is a vision library for GeniCam technology based cameras.

The Graphical User Interface and Numerical Template Library is part of the Spectroscopic Data Systems (SDS) which is written in C++ and uses multi-threaded event-driven graphical communications to a single `X11` server via native `Xlib` calls in the same application.

The camera has a single RJ45 connector and powered over Ethernet link with a separate standard power supply. As the power consumption may grow high during continuous CCD readouts, the temperature of the camera may grow up as high as to 60C, hence, the camera is equipped with a custom made heat sink to reduce any thermal noise on the CCD during integration.

The camera is not equipped with a mechanical shutter, but is using a global electronic shutter. The exposure times are limited to the range of $1\,\mu\text{s} - 1\,\text{s}$. In the case of faint targets when 1 s integration time is not sufficient to get enough light, a special accumulation mode is used where a specified number of short exposures are summed up into the resulting image for further analysis of the target position.

The communication with the VATT telescope control system (TCS) is implemented with a dedicated Internet socket which accepts a number of interface commands. The PEPSI VATT control interface uses the commands to point the telescope to a target with the specified equatorial coordinates, to apply a small guiding corrections in RA/Dec, and to obtain status information of the current position of the telescope and its environment. The PEPSI VATT adapter is mounted in the fixed position in the Cassegrain focus flange with no de-rotator being used during observations, therefore, the guiding CCD offset corrections in XY of the Alt/Az frame are always converted into the equatorial coordinate system as required by the TCS (Fig. 7b).

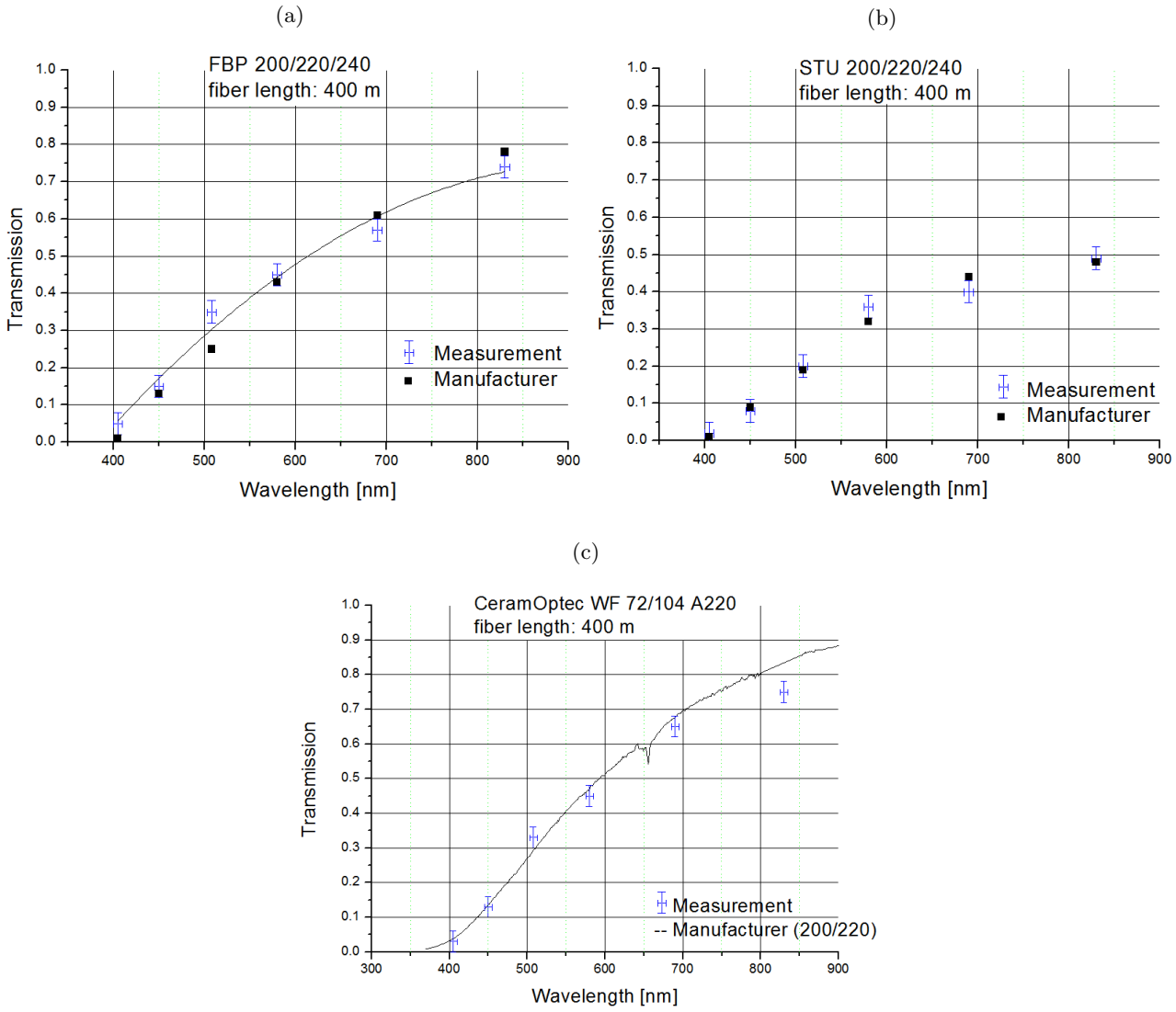

Figure 6: Transmission for the three measured fibres compared to values from the manufacturers.

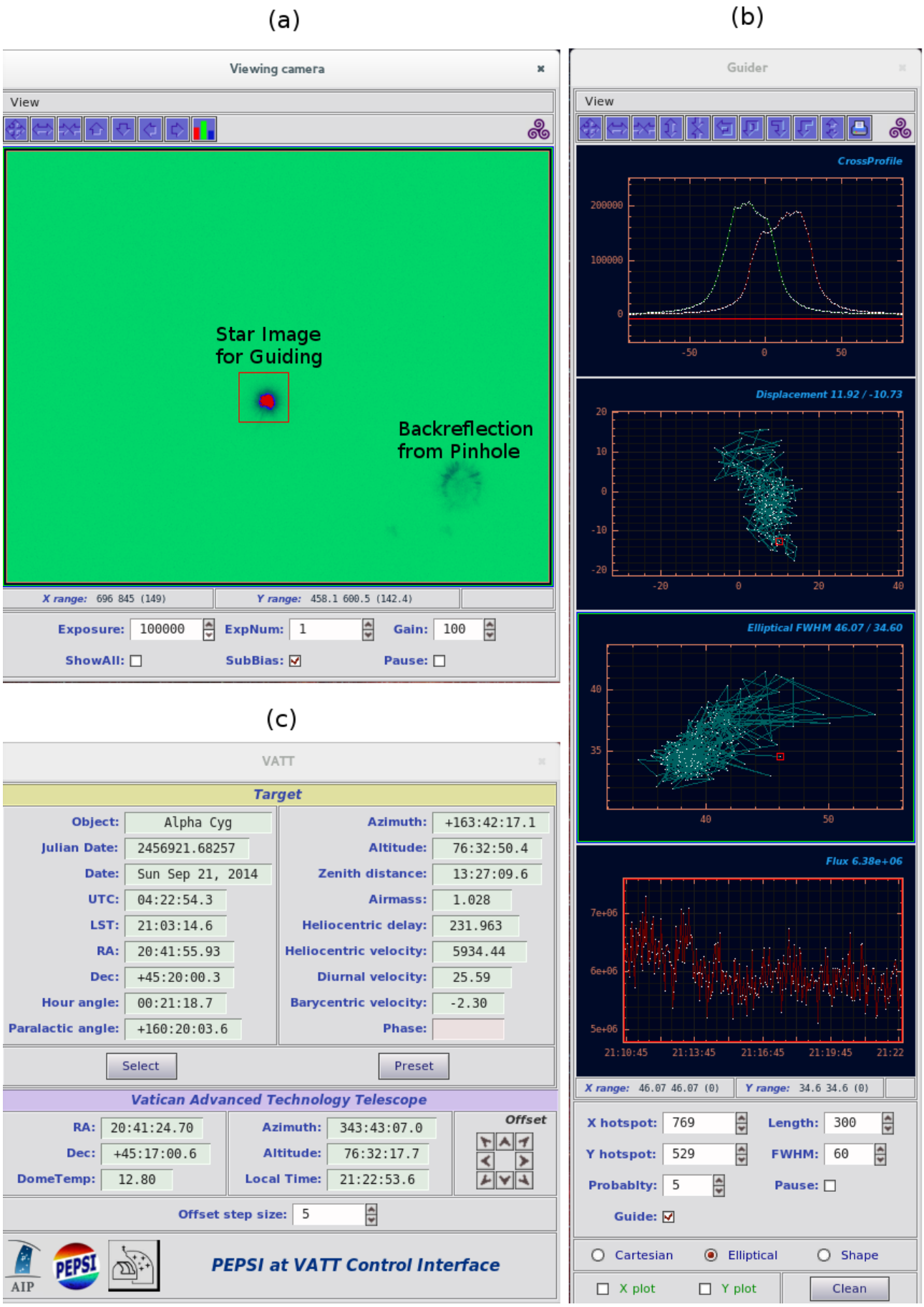

Figure 7: The Graphical Interface to control VATT by presetting telescope to the selected star (c) and guiding on the direct reflected guider image (at the center of the image, b). The back-reflected fiber pinhole image is seen at the bottom right part of the image (a).

The observing targets are stored and subsequently selected from the catalog stored as the FITS Binary table and managed by a separate graphical application (Fig. 7c). Alternatively the observing target can be retrieved from the observing blocks of the PEPSI control program. The observing catalog application has a capability to retrieve coordinates and other attributes from SIMBAD database via Internet socket, as well as to display visibility plot of the selected targets. Once the next observing target is selected, the observer can initiate the telescope to slew to the new position. Once the new target appears on the CCD camera at about its center, the observer can start guiding on the target. In case the target appears too far from the CCD center due to pointing errors, its position can be corrected by GUI buttons to move the star in Alt/Az coordinate system closer to the CCD center.

The guiding is done on the direct-reflected image of the observing target and the back-reflected image from the mirrored pinhole of the 200 μm fiber is merely used to verify that the star is well centered on the pinhole (Fig. 7a). This configuration is achieved with a gray beam-splitter which has a mirrored wedge on one side to offset the back-reflected image on diagonal of the CCD. The direct-reflected guider image takes a few percent of the target light. The guider application keeps the target at the specified hotspot position on the CCD by applying small corrections to the TCS to ensure that the star is well centered on the pinhole. The pinhole position can be otherwise interactively modified especially after mounting and dismounting the adapter in the Cassegrain focus.

Prior to the image processing to obtain the guiding offsets, the raw CCD image has to be de-trended to avoid any gradients due to illumination and thermal effects. The background surface is removed with two-pass iterations in CCD columns first, then in rows. The image is first partitioned in 128 stripes in columns where the median value for each stripe is calculated. A spline fit of the specified smoothing factor through these 128 background estimates is used to evaluate and subsequently subtract from every column of the CCD image. Then, the same procedure is repeated but in CCD rows since the background gradient may have bi-directional slope.

A Gaussian windowed center of gravity is used to determine the offset of the direct-reflected image of the star from the hotspot position. A typical FWHM of the Gaussian window is about $7'' - 10''$ on sky and can be alternated depending on the seeing conditions. The use of the windowed function is justified as it gives a more precise position of the source via iterative process of re-adjusting of the position of the window function to the final position and eliminates any side effects which may take place in the field of view. The second moment of the gravity center gives estimates of the FWHM of the seeing profile and its covariance from which the Cartesian or elliptical seeing conditions are calculated. The finite width of the Gaussian window affects the FWHM of the seeing profile as they added in reciprocal quadratures as the result of the product of two Gaussian profiles, hence, the window function FWHM has to be excluded from the final estimate of the width.

When calculating the first moment of the center of gravity, we also use the variances of the photon noise with the assumption of the Poisson noise distribution for each CCD pixel. The variances, properly scaled with the Gaussian window function, allow for the errors and covariance estimate of the determined center of gravity. Subsequently, as the guider camera collects a number of such estimates, we calculate the mean offset and covariance matrix of the random variables correlated in XY, from which we derive the total accumulated offset distance and its variance. As the next step, we evaluate its statistical significance with the F-test. If the statistical significance is lower than specified level (a typical False Alarm Probability (FAP) level is $10^{-3} - 10^{-5}$), we continue to collect more guider images and accumulate more accurate mean center of gravity estimate. Once it becomes statistically more significant, then the correction in XY are applied and the accumulation of the mean offset is started over. If we want more frequent corrections of the guide star, then we need to rise the level of FAP, and the opposite is true, so that with the lower FAP level the guiding offset are applied less frequently.

3. OBSERVATIONS

The observations using the VATT are divided into several runs per semester of 7–10 nights each, usually during bright time. Bright targets are chosen to get data with high SNR at highest possible resolution. However, also some fainter targets such as θ^1 Ori C (magnetic brake candidate) were observed. Additionally, 10 nights of simultaneous observations where made on Capella to cover the rotation period of the secondary component. This system is of particular interest, since both components are evolved stars. The secondary, however, has just started the move from the main sequence through the Hertzsprung gap towards the AGB. It shows the higher

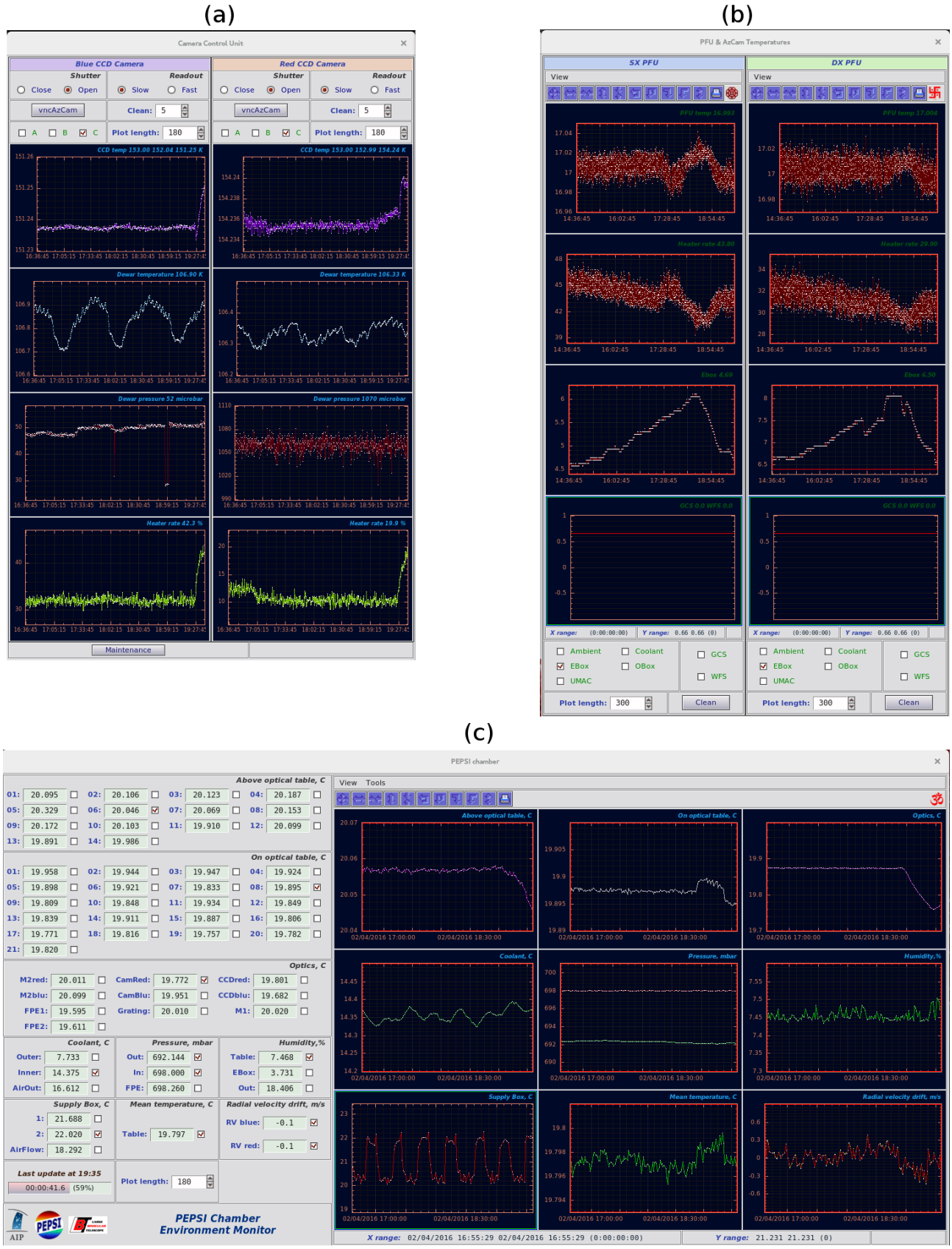

Figure 8: The environmental data dispayed via the PEPSI control program. (a) shows the temperature and pressure value for the blue and red CCDs. (b) are the values of the PFUs and (c) shows the environment of the PEPSI spectrograph chamber.

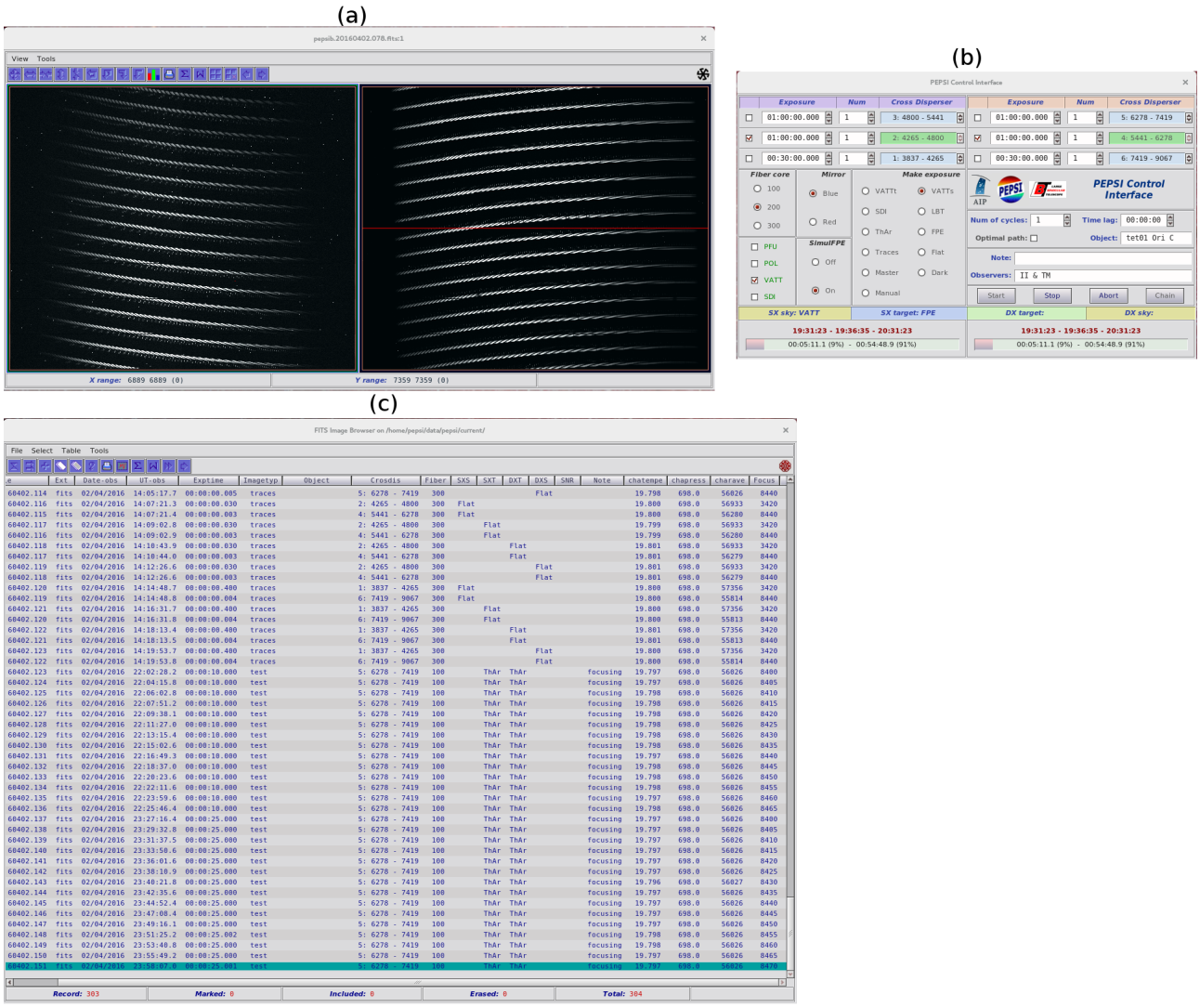

Figure 9: The windows for PEPSI set-up and data visualization via the PEPSI control program. (a) shows the raw fits frames and allows to use and plot regions of the frame in x and y. The window (b) is to choose the proper configuration for the exposure (cross-disperser, exposure time etc.) and (c) collects all frames in a table from where they can be loaded.

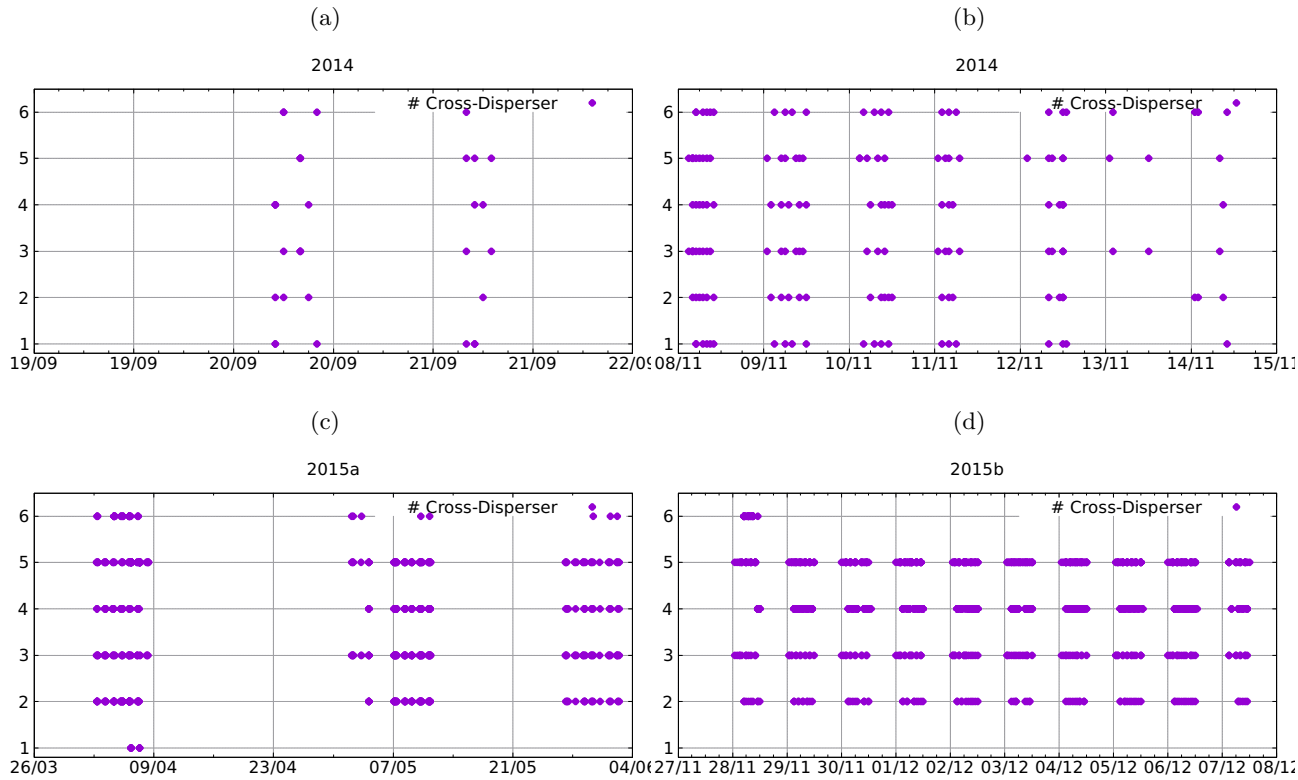

Figure 10: Observations vs. time plotted for all six cross-disperser for (a) semester 2014 A, (b) semester 2014 B, (c) semester 2015 A and (d) semester 2015 B.

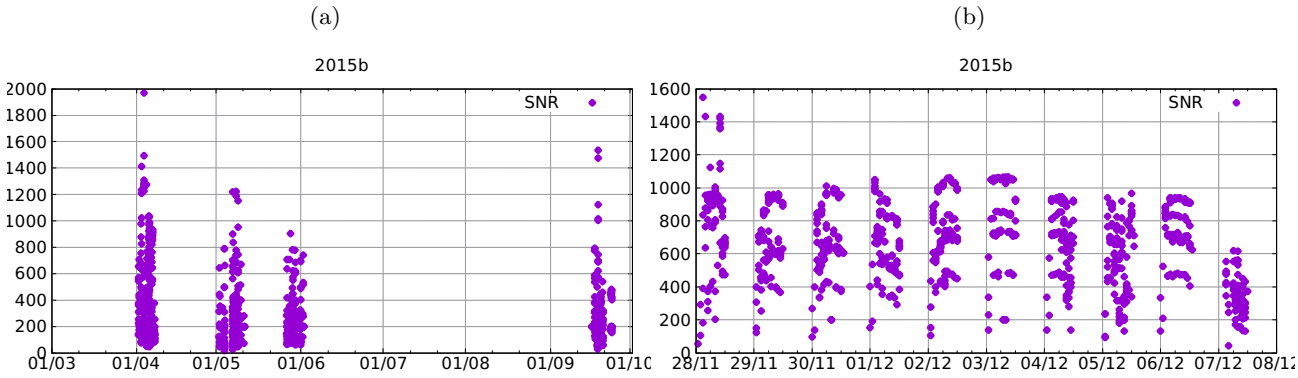

Figure 11: Signal-to-noise ratio vs. time for observations in (a) semester a 2015 and (b) semester b 2015.

lithium surface abundance since convective mixing has not affected it yet. The masses of both components are very precisely determined,[5] such that analysis of the evolution where performed with high accuracy.[2] Hence, dense and high-resolution of spectra for Doppler imaging of the secondary Hertzsprung gap star where obtained.

In Fig. 10 we show some statistics of obtained observations with PEPSI linked to VATT in dependence of the used cross-dispersers. Due to the 450m of fibre in between, measurements in the blue region (CD I) where not continued in 2015.

We show the signal-to-noise ratio of the measurement of 2015 in Fig. 11. Again, the fibre limits signal-to-noise in the blue, therefore high values are only obtained in the red spectral regions.

4. FUTURE WORK AND CONCLUSION

A new image slicer for PEPSI is in construction and will provide an additional stack for the VATT fibre. The VATT fibre will be removed from the PFU and connected to a fibre switch near the spectrograph. From that switch, a dedicated fibre is attached to the transformation optics at the spectrograph input which feeds the image slicer. Using the 200μm fiber but filling the space normally used for the two individual spectra from the LBT SX and DX telescopes, this will give a resolution comparable to the ultra-high-resolution mode usually provided using the 100μm fibres. It will also increase throughput since re-coupling inside the PFU is no longer necessary.

REFERENCES

[1] Strassmeier, K. G., Ilyin, I., Järvinen, A., Weber, M., Woche, M., Barnes, S. I., Bauer, S.-M., Beckert, E., Bittner, W., Bredthauer, R., Carroll, T. A., Denker, C., Dionies, F., DiVarano, I., Döscher, D., Fechner, T., Feuerstein, D., Granzer, T., Hahn, T., Harnisch, G., Hofmann, A., Lesser, M., Paschke, J., Pankratow, S., Plank, V., Plüschke, D., Popow, E., and Sablowski, D., "PEPSI: The high-resolution échelle spectrograph and polarimeter for the Large Binocular Telescope," *Astronomische Nachrichten* **336**, 324 (May 2015).

[2] Torres, G., Claret, A., Pavlovski, K., and Dotter, A., "Capella (α Aurigae) Revisited: New Binary Orbit, Physical Properties, and Evolutionary State," *ApJ* **807**, 26 (July 2015).

[3] Sablowski, D. P., Plüschke, D., Weber, M., Strassmeier, K. G., and Järvinen, A., "Comparing modal noise and FRD of circular and non-circular cross-section fibres," *Astronomische Nachrichten* **337**, 216 (Feb. 2016).

[4] Butov, O., Golant, K., Tomashuk, A., Van Stralen, M., and Breuls, A., "Refractive index dispersion of doped silica for fiber optics," *Optics Communications* **213**(4), 301–308 (2002).

[5] Weber, M. and Strassmeier, K. G., "The spectroscopic orbit of Capella revisited," **531**, A89 (July 2011).